Ocean Surface Wave Optical Roughness – Analysis of Innovative Measurements

Michael L. Banner
School of Mathematics and Statistics
The University of New South Wales
Sydney 2052, Australia
Tel : (+61-2) 9385-7071 fax: (+61-2) 9385-7123 email: m.banner@unsw.edu.au

Russel P. Morison
School of Mathematics and Statistics
The University of New South Wales
Sydney 2052, Australia;
Tel : (+61-2) 9385-7064 fax: (+61-2) 9385-7123 email: r.morison@unsw.edu.au

Award Number: N00014-11-1-0054

LONG-TERM GOALS

We are part of a multi-institutional research team funded by the ONR-sponsored Radiance in a Dynamic Ocean (RaDyO) program. The primary research goals of the program are to (1) examine time-dependent oceanic radiance distribution in relation to dynamic surface boundary layer (SBL) processes; (2) construct a radiance-based SBL model; (3) validate the model with field observations; and (4) investigate the feasibility of inverting the model to yield SBL conditions. Our goals are to contribute innovative measurements, analyses and models of the sea surface roughness at length scales as small as a millimeter. This characterization includes microscale and whitecap breaking waves.

The members of the research team are

Michael Banner, School of Mathematics, UNSW, Sydney, Australia

Johannes Gemmrich, Physics and Astronomy, UVic, Victoria, Canada

Russel Morison, School of Mathematics, UNSW, Sydney, Australia

Howard Schultz, Computer Vision Laboratory, Computer Science Dept, U. Mass., Mass

Christopher Zappa, Lamont Doherty Earth Observatory, Palisades, NY

OBJECTIVES

Nonlinear interfacial roughness elements - sharp crested waves, breaking waves as well as the foam, subsurface bubbles and spray they produce, contribute substantially to the distortion of the optical transmission through the air-sea interface. These common surface roughness features occur on a wide range of length scales, from the dominant sea state down to capillary waves. Wave breaking signatures range from large whitecaps with their residual passive foam, down to the ubiquitous centimeter scale

Report Documentation Page

Form Approved
OMB No. 0704-0188

1. REPORT DATE	2. REPORT TYPE	3. DATES COVERED
30 SEP 2011		

4. TITLE AND SUBTITLE	5a. CONTRACT NUMBER
Ocean Surface Wave Optical Roughness - Analysis of Innovative Measurements	5b. GRANT NUMBER
	5c. PROGRAM ELEMENT NUMBER
6. AUTHOR(S)	5d. PROJECT NUMBER
	5e. TASK NUMBER
	5f. WORK UNIT NUMBER
7. PERFORMING ORGANIZATION NAME(S) AND ADDRESS(ES) **The University of New South Wales,School of Mathematics and Statistics,Sydney 2052, Australia, ,**	8. PERFORMING ORGANIZATION REPORT NUMBER
9. SPONSORING/MONITORING AGENCY NAME(S) AND ADDRESS(ES)	10. SPONSOR/MONITOR'S ACRONYM(S)
	11. SPONSOR/MONITOR'S REPORT NUMBER(S)

12. DISTRIBUTION/AVAILABILITY STATEMENT
Approved for public release; distribution unlimited.

13. SUPPLEMENTARY NOTES

14. ABSTRACT

15. SUBJECT TERMS

16. SECURITY CLASSIFICATION OF:			17. LIMITATION OF ABSTRACT	18. NUMBER OF PAGES	19a. NAME OF RESPONSIBLE PERSON
a. REPORT	b. ABSTRACT	c. THIS PAGE			
unclassified	**unclassified**	**unclassified**		**9**	

microscale breakers that do not entrain air. There is substantial complexity in the local wind-driven sea surface roughness microstructure, including very steep nonlinear wavelets and breakers. Traditional descriptors of sea surface roughness are scale-integrated statistical properties, such as significant wave height, mean squared slope (e.g. Cox and Munk, 1954) and breaking probability (e.g. Holthuijsen and Herbers, 1986). Subsequently, spectral characterisations of wave height, slope and curvature have been measured, providing a scale resolution into Fourier modes for these geometrical sea roughness parameters. More recently, measurements of whitecap crest length spectral density (e.g. Phillips et al, 2001, Gemmrich et al., 2008) and microscale breaker crest length spectral density (e.g. Jessup and Phadnis, 2005) have been reported.

Our effort seeks to provide a more comprehensive description of the physical and optical roughness of the sea surface. We will achieve this through the analysis of our suite of comprehensive sea surface roughness observational measurements within the RADYO field program. These measurements are designed to provide optimal coverage of fundamental optical distortion processes associated with the air-sea interface. In our data analysis, and complementary collaborative effort with RaDyO modelers, we are investigating both spectral and phase-resolved perspectives. These will allow refining the representation of surface wave distortion in present air-sea interfacial optical transmission models.

APPROACH

We build substantially on our accumulated expertise in sea surface processes and air-sea interaction. We are working within the larger team (listed above) measuring and characterizing the surface roughness. This team is contributing the following components to the primary sea surface roughness data gathering effort in RaDyO:

- polarization camera measurements of the sea surface slope topography, down to capillary wave scales, of an approximately 1m x 1m patch of the sea surface (see Figure 1), captured at video rates. [Schultz, Zappa]
- co-located and synchronous orthogonal 75 Hz linear scanning laser altimeter data to provide spatio-temporal properties of the wave height field (resolved to O(0.5m) wavelengths) [Banner, Morison]
- high resolution video imagery to record whitecap data from two cameras, close range and broad field [Gemmrich]
- fast response, infrared imagery to quantify properties of the microscale breakers, and surface layer kinematics and vorticity [Zappa]
- air-sea flux package including sonic anemometer to characterize the near-surface wind speed and wind stress [Zappa]

The team's envisaged data analysis effort includes: detailed analyses of the slope field topography, including mean square slope, skewness and kurtosis; laser altimeter wave height and large scale wave slope data; statistical distributions of whitecap crest length density in different scale bands of propagation speed and similarly for the microscale breakers, as functions of the wind speed/stress and the underlying dominant sea state. Our contributions to the modeling effort will focus on using RaDyO data to refine the sea surface roughness transfer function. This includes the representation of nonlinearity and breaking surface wave effects including bubbles, passive foam, active whitecap cover and spray, as well as micro-breakers.

WORK COMPLETED

Our effort in FY11 comprised further analysis of the suite of atmospheric fluxes and sea surface roughness measurements gathered from FLIP during the RaDyO field experiments in the Santa Barbara channel during September 5-27, 2008 and Hawaii during August 23-September 16, 2009. We participated actively in refining the analysis and validation of the polarimetric and wave breaking data. We also carried out further processing, validation and archiving of our scanning lidar data collocated with our partner investigators' high resolution polarimeteric, infrared and optical imaging. This data provides the large scale wave geometry (height and slope) throughout the observational periods.

RESULTS

Figure 1 below shows the instrumentation deployed in the field measurement phase. Banner/Morison deployed two orthogonal line scanning lidars, synchronized for zero crosstalk. The lidars were positioned on the boom so that their intersection point was within the common footprint of the polarimetric (Schultz), infrared (Zappa) and visible (Gemmrich) imagery cameras which were measuring small-scale surface roughness features and breaking waves. The scanning lidars provided data on the height and local directional slope of the gravity waves, characterizing the background environment experienced by the very short wind waves that comprise the sea surface microstructure. This information allows accurate phasing of the polarimetric, infrared and visible camera imagery of the sea surface microstructure with respect to the underlying dominant wind waves.

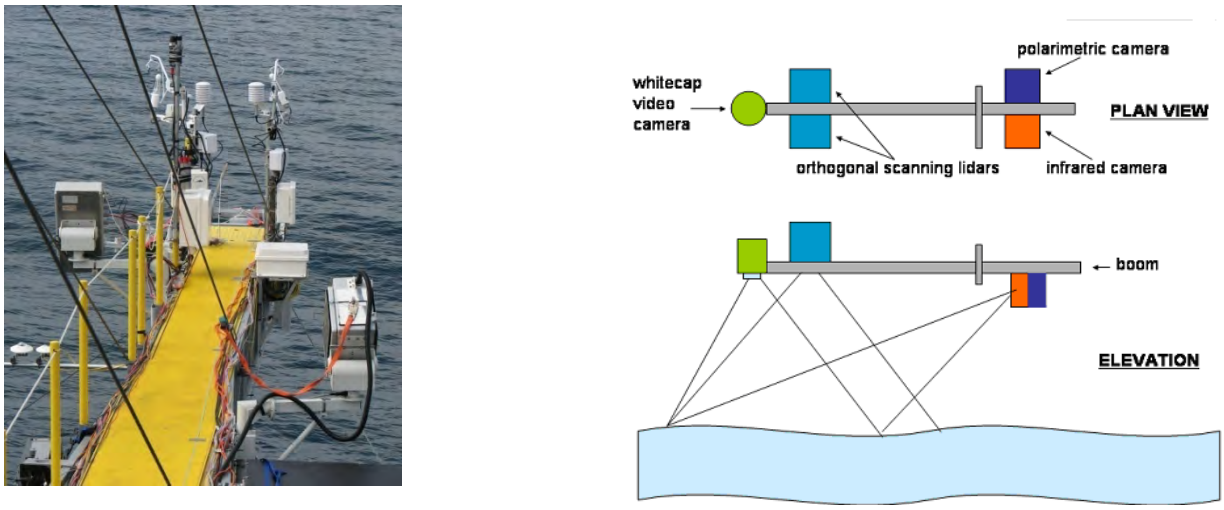

Figure 1. The left panel shows the instrumentation set-up deployed from the FLIP starboard boom. The right panel shows a schematic of instrumentation packages deployed. The end of the boom was about 8m above the mean water level. The approximate field of view of the various instruments is shown. A second wide angle whitecap video camera was mounted on FLIP well above the boom to image the larger whitecaps.

Zappa deployed his infrared/visible camera system and his environmental monitoring system (sonic anemometer, water vapor sensor, relative humidity/temperature probe, motion package, pyranometer and pyrgeometer). Gemmrich deployed 2 video visible imagery cameras. One camera was mounted on the main boom next to our other instrumentation packages, the second camera was mounted higher up to view larger scale breaking events. Schultz deployed an instrument package located on the boom that includes a polarimetric camera imaging the very small-scale waves. The individual data acquisition systems were synchronized to GPS accuracy which allowed the various data sets to be interrelated to within 0.1 seconds.

Air-sea fluxes

Time series of momentum (wind stress), sensible heat, and water vapor direct covariance fluxes during the Santa Barbara Channel study are shown in the left panel of Figure 6. Also shown are the TOGA-COARE model bulk fluxes (Fairall et al. 2003). Diurnal processes were the origin of most of the variability in the atmospheric and oceanic forcing. The momentum, sensible heat and latent heat fluxes all show a diurnal cycle similar to the wind speed. The mean and standard deviation of the momentum flux for the whole experiment was 0.070 ± 0.061 N m^{-2}, while the momentum flux during the three regimes 0.062 ± 0.064 N m^{-2} (Days 257-259), 0.104 ± 0.062 N m^{-2} (Days 260-263), and 0.042 ± 0.035 N m^{-2} (Days 264-268) respectively. The most significant diurnal process is the heating and cooling of the ocean surface. The surface ocean is heated during the day by incident solar radiation. At night, when solar radiation is nonexistent, infrared radiation, evaporation, and sensible heat fluxes cool the ocean surface. These processes vary through the diurnal cycle and cause subsequent processes that change the transport of heat, mass, and momentum across the air-sea interface. The diurnal barometric pressure changes are small. Thus, the time series of direct covariance measurements are close to a uniform daily mean and banded around variability caused by noise and diurnal forcing.

The mean and standard deviation of the sensible and latent heat direct covariance fluxes were -13.9 ± 10.7 W m^{-2} and -33.9 ± 21.8 W m^{-2}. Note that the standard deviations of the measured half-hour direct covariance fluxes are often as large as the mean fluxes. For Days 258-263, the mean sensible heat flux was -20.8 ± 8.8 W m^{-2}, the mean latent heat flux was -45.6 ± 17.2 W m^{-2}, and the mean net cooling at night was -125.6 ± 38.5 W m^{-2}. During regime three between Days 264-268, the mean sensible heat flux was -6.4 ± 7.8 W m^{-2}, the mean latent heat flux was -21.7 ± 19.9 W m^{-2}, and the mean net cooling at night was -89.3 ± 16.5 W m^{-2}. The peak warming throughout the experiment ranged between 600 W m^{-2} and 750 W m^{-2}.

Time series of momentum (wind stress), sensible heat, and water vapor direct covariance fluxes during the central Pacific Ocean study south of Hawaii are shown in the right panel of Figure 2. Similar to the wind speed, the momentum flux shows a slow decrease from 0.16 N m^{-2} at the beginning of the experiment to 0.10 N m^{-2} at the end. The average momentum flux for the whole experiment was 0.118 ± 0.041 N m^{-2}. Again, the most significant diurnal process is the heating and cooling of the ocean surface. The mean and standard deviation of the sensible and latent heat direct covariance fluxes were -15.1 ± 5.46 W m^{-2} and -126.9 ± 32.2 W m^{-2}. The mean net cooling at night throughout the experiment was -190.2 ± 43.35 W m^{-2}. The peak warming throughout the experiment ranged between 600 W m^{-2} and 780 W m^{-2}. Note that on Day 253, rain contaminated all the direct covariance fluxes, including the net heat flux.

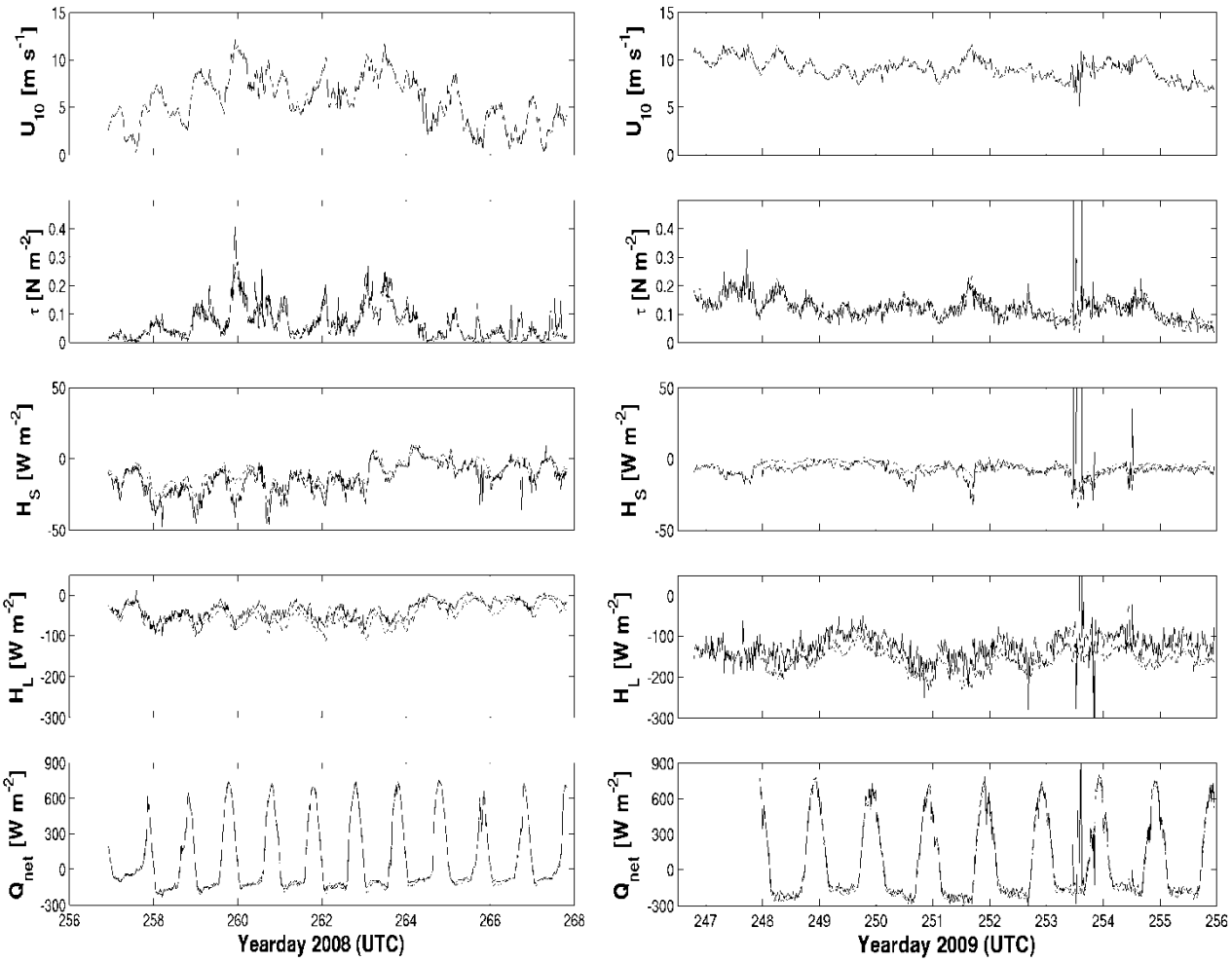

Figure 2. Time series of wind speed U_{10}, momentum flux (wind stress) τ, sensible heat flux H_s, latent heat flux H_l, and net heat flux Q_{net}, during the Santa Barbara Channel experiment (left panel) and during the central Pacific Ocean experiment south of Hawaii (right panel). Solid lines use direct covariance measurements and dashed lines use TOGA-COARE bulk fluxes.

Short ocean wave microstructure

Figure 3 below shows examples of observed wavenumber-frequency slope spectral slices for both the along-wind and cross-wind directions, determined from the polarimeter slope field data from the Santa Barbara Channel experiment. Two-sided spectra provide information on the direction of propagation. These short wave spectra capture data at comparable scales as previously in Hara et al. [1998], but without any instrument disturbances to the sea surface.

Two cases are shown, one for weak winds (U_{10} ~ 2 m/s) and one for stronger winds (U_{10} ~ 9 m/s). These figures show that the wave slope energy follows the linear dispersion relation at low wavenumbers both in the wind direction and in the cross-wind direction. As the wavenumber increases, the wave slope energy can deviate systematically from the linear dispersion relation. This

migration of higher wavenumber components off the dispersion curve is likely due to background currents, as the dispersion relation connecting the observed and intrinsic wave frequencies contains an additive Doppler-shift offset term $\underline{U}.\underline{k}$, where $\underline{U}$ is the velocity of the background current and $\underline{k}$ is the wavenumber vector. We are investigating the most likely source of the apparent Doppler shift, the ambient current, which is known from synchronized upward-looking Acoustic Doppler Current Profiler (ADCP) data recorded and provided by the Scripps group.

Our ongoing analysis is also investigating further details of these spectra, including the nonlinearity of the short waves and their depth of modulation by the dominant wind sea. The effects of these surface roughness features on the subsurface light field are currently being investigated with several RaDyO collaborators.

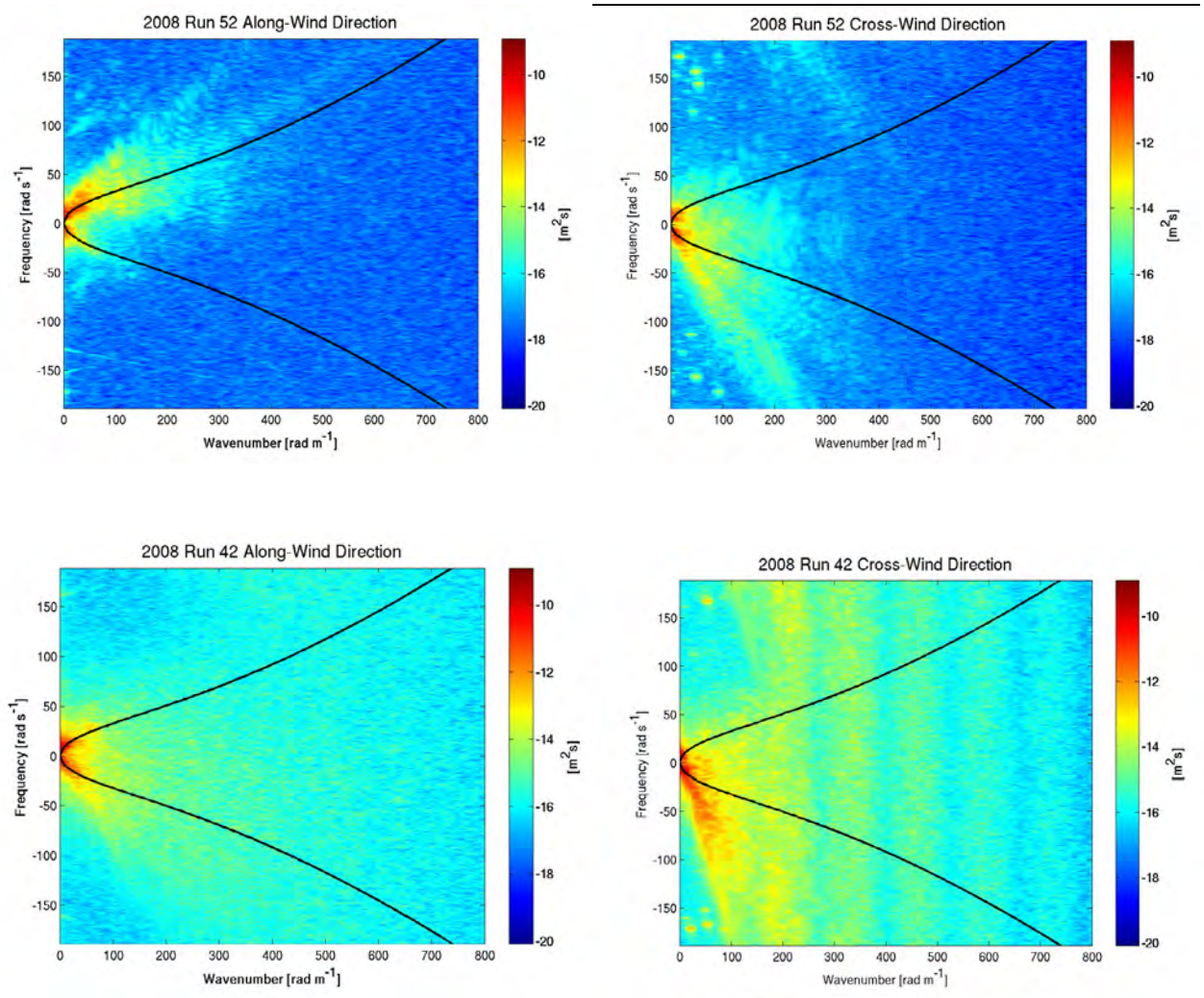

Figure 3. Wavenumber-frequency slope spectral slices from the polarimeter data in the along-wind (Left) and cross-wind (Right) directions during the RaDyO Santa Barbara Channel Experiment with a wind speed of 2.0 m s^{-1} (upper panels) and 9.3 m sec^{-1} (lower panels). The superimposed continuous white curve is the linear dispersion relation for zero mean current.

Breaking Crest Length Distributions

We measured breaking crest length density $\Lambda(c_b)$ distributions during both the Santa Barbara Channel and the Hawaii experiments with our suite of video and infrared cameras mounted on R/P FLIP. The scale of wave breaking during both field experiments ranged from microbreakers to small-scale breakers with air entrainment to breaking dominant waves. These data were analyzed in terms of breaking crest length density, foam coverage and whitecap persistence. Results on the breaking crest length distribution $\Lambda(c_b)$ independent of direction, obtained by the discrete breaker tracking decomposition method, are shown in Figure 4 for RaDyO experiments in Santa Barbara Channel and in the central Pacific Ocean south of Hawaii. Comparison of $\Lambda(c_b)$ determined from our visible and infrared imagery (not shown here) at a similar wind speed of 10 m s^{-1} shows that the infrared better captures the microbreaking at smaller breaking scales, confirming that these roughness features are important to the breaking distribution.

From Figure 4 it is also seen that small-scale wave breaking was significantly less in the central Pacific Ocean south of Hawaii than in Santa Barbara Channel. The maximum of $\Lambda(c_b)$ is in the intermediate to short wave range, with a variation in the absolute values below this range. However, the slope of the family of Λ curves for longer waves is close to the Phillips (1985) canonical form $\Lambda(c) \sim c^{-6}$. In the Santa Barbara Channel, the overall level of Λ fluctuated by more than 1 order of magnitude, roughly following the fluctuations in wind stress (see Figure 2). The wave height and wind speed during the Hawaii experiment fluctuated less, and were comparable to the more energetic periods of the Santa Barbara Channel experiment. The peak values of the Λ distributions of the two experiments are similar. However, the slopes of the distributions are noticeably different, indicating a stronger contribution of larger-scale breakers during the Santa Barbara Channel experiment.

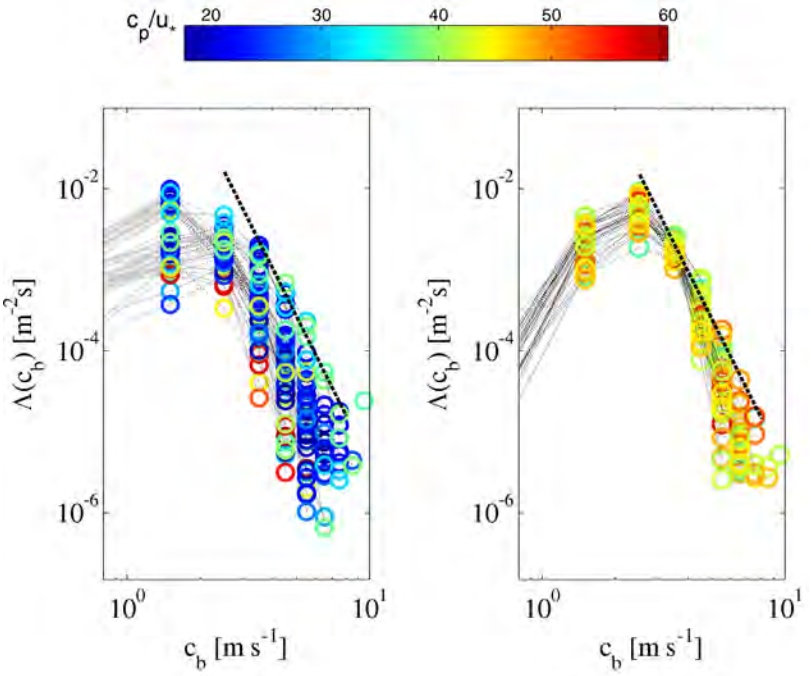

Figure 4. Distributions of breaking crest length spectral density against breaker speed c_b from optical imagery during the Santa Barbara Channel (left) and Hawaii (right) experiments. Note that the wave age (c_p/u_*) shows young wind seas in Santa Barbara Channel compared to old wind seas south of Hawaii. The dashed line represents the c^{-6} dependence predicted by Phillips (1985).

IMPACT/APPLICATIONS

This effort will provide a far more detailed characterization of the wind driven air-sea interface, including wave breaking (whitecaps and microscale breaking). This is needed to provide more complete parameterizations of these processes, which will improve the accuracy of ocean optical radiative transfer models and trans-interfacial image reconstruction techniques.

REFERENCES

Cox, C.S. and Munk, W.H., 1954: Measurements of the roughness of the sea surface from photographs of the sun glitter. J. Opt. Soc. Am. 44, 838-850.

Fairall, C. W., E. F. Bradley, J. E. Hare, A. A. Grachev, and J. B. Edson (2003), Bulk parameterization of air-sea fluxes: Updates and verification for the COARE algorithm, *J. Climate, 16,* 571-591.

Gemmrich, J.R., M.L. Banner and C. Garrett, 2008: Spectrally resolved energy dissipation and momentum flux of breaking waves. J. Phys. Oceanogr. 38, 1296-1312.

Hara, T., E. J. Bock, J. B. Edson, and W. R. McGillis (1998), Observation of short wind waves in coastal waters, *Journal of Physical Oceanography*, *28*(7), 1425-1438.

Holthuijsen, L.H., and T.H.C. Herbers, 1986: Statistics of breaking waves observed as whitecaps in the open sea, Journal of Physical Oceanography, 16, 290-297.

Jessup, A.T. and Phadnis, K.R. 2005 Measurement of the geometric and kinematic properties of microscale breaking waves from infrared imagery using a PIV algorithm. Meas. Sci. Technol. 16, 1961-1969.

Phillips, O. M. (1985), Spectral and statistical properties of the equilibrium range in wind-generated gravity waves, *Journal of Fluid Mechanics, 156,* 505-531.

Phillips, O.M., Posner, F.L. and Hanson, J.P., 2001: High resolution radar measurements of the speed distribution of breaking events in wind-generated ocean waves: surface impulse and wave energy dissipation rates. J. Phys. Oceanogr., 31, 450–460.

PUBLICATIONS

Howard Schultz, Chris J. Zappa, Michael L. Banner, Andres Corrada-Emmanuel and Larry Pezzaniti (2008) "A Method for Recovering the Two-dimensional slope field of the Ocean Surface Waves Using an Imaging Polarimeter", 2008 AGU Ocean Sciences Meeting, Orlando, FL March 2-7, oral presentation. [Published]

Zappa, C.J., M.L. Banner, H. Schultz, A.Corrada-Emmanuel, L.B. Wolff and J. Yalcin, 2008: Retrieval of Short Ocean Wave Slope Using Polarimetric Imaging. Measurement Science and Technology. Measurement Science and Technology, 19, 055503, pp 13, April 2008 [published, refereed].

Gemmrich, J.R., M.L. Banner and C. Garrett, 2008: Spectrally resolved energy dissipation and momentum flux of breaking waves. J. Phys. Oceanogr. 38, 1296-1312. [published, refereed]

Zappa. C.J., J.R. Gemmrich, R. P. Morison[3], H. Schultz[4], M. L. Banner[5], D.A. LeBel[1], and T. Dickey[6] An overview of sea state conditions and air-sea fluxes during RaDyO. J. Geophys. Res. [in revision, refereed]